Materials Research, Vol. 11, No. 3, 281-288, 2008

Study of the Dimensions of Double-Torsion Test Specimens

Maria da Consolação Fonseca de Albuquerque*[a]*, José de Anchieta Rodrigues*[b]

[a]*Departamento de Engenharia Civil, Universidade Estadual Paulista – UNESP, Alameda Bahia, 550 – Norte, 15385-000 Ilha Solteira - SP, Brazil*
[b]*Departamento de Engenharia de Materiais, Universidade Federal de São Carlos – UFSCar, Via Washington Luis, Km 235, 13565-905 São Carlos - SP, Brazil*

Received: March 5, 2008; Revised: August 20, 2008

Double-torsion tests were carried out to ascertain whether a thin test specimen would affect the results of this test. The tests involved two test specimen sizes, one with a thickness five-fold greater than the particle size of the material and the other with a three-fold greater thickness. The width of both test specimens was ten times that of their thickness and their length was double their width. The material utilized was an alumina-based refractory castable without cement. It is important to ascertain the influence of the thickness of double-torsion test specimens when materials with a coarse microstructure are involved. Otherwise, test specimens would have to be very large, rendering the experimental procedure difficult, as in the case of the size of sintering furnaces and the size of accessories for the test. This study shows that test specimens with lower thicknesses are representative when one analyzes the calibration curve of the compliance, the length of the crack at which the break occurred (critical crack length), and the shapes of the R-curve and of the load (P) vs. displacement curves. However, the analysis of the mean values of R ($\overline{R}$), obtained by the arithmetic average of the R values in the section of stable crack propagation and the total fracture energy (γ_{wof}), showed that these values are dependent on the size of the test specimens, indicating that this subject deserves further investigation.

Keywords: *mechanical properties, double-torsion test, fracture mechanics, refractory castable*

1. Introduction

Ceramic materials are brittle, with low toughness. The mechanical behavior of these materials is described by the theory of linear elastic fracture mechanics (LEFM), which quantitatively describes the transformation of an intact structural component into a fractured one through the growth of a crack.

More in-depth studies of ceramic materials usually involve measurements of the crack growth rate and fracture toughness and determination of their R-curve, among other characteristics. Obtaining some of these measures requires the condition of stable crack propagation. This condition may be difficult to achieve with some test geometries, but the geometry of the double-torsion test specimen eliminates this difficulty.

The double-torsion test is a typical test in fracture mechanics used for subcritical crack growth[1], i.e., under the condition of stable crack propagation.

The concept of the double-torsion configuration was introduced by Outwater and Gerry[2,3]. Several authors[1-29] have discussed the development and some problems of this technique. In the last four decades, the double-torsion method has been widely employed to obtain subcritical crack growth in studies of the dependence of crack propagation velocity on the applied K_I value. However, no standard has yet been established for this test with ceramic materials.

In the literature on other tests, one commonly finds that the smallest dimension of a test specimen should be at least five times the size of the diameter of the largest grain, in order to have a test specimen that is representative of the material's microstructure. The confirmation that a test specimen with a thickness of less than five times the largest particle diameter does not impair the quality of the double-torsion test is important when materials with a coarse microstructure are involved, as in the case of refractories. Otherwise, test specimens would have to be very large, making the experimental procedure difficult, as in the case of the size of laboratory sintering furnaces and the size of the accessories for the test.

In this study, we conducted stable crack propagation tests in a double-torsion arrangement on alumina-based refractory castable without cement with a maximum particle size of two millimeters. The width of the test specimens was ten times their thickness and their length was twice their width. Test specimens were prepared in two sizes, one with a thickness three times the size of the largest particle of the raw materials, and the other five times that size. Our purpose was to ascertain whether the results of this technique are affected by the size of the test specimens when the thickness of the sample is relatively small. This is an extremely important point when one wishes to study a refractory composed of large particles using the double-torsion test, since a geometry whose width should be much greater than its thickness and whose length should be twice the width would result in very large test specimens, leading to the aforementioned difficulties.

The aim in this study was to produce thin test specimens whose thickness would still be compatible with some representativeness of the fracture area, which is why no specimens were prepared with thicknesses of less than 3 times the size of the largest particle.

The following properties were characterized: apparent porosity, apparent specific mass of the solid part, apparent specific mass, Young's modulus, stable crack propagation, and R-curve.

2. Preparation of the Test Specimens

The material studied in this work was a high-alumina refractory castable without cement, with a maximum grain size of 2 mm. Table 1 shows the formulation of this castable. The raw materials utilized were two types of alumina, calcined and electrofused, and citric acid as dispersant (0.05% in weight).

The castable's particle distribution was calculated based on Andreasen's particle packing model, using a particle size distribution coefficient, q, of 0.21 for the castable. This distribution was calculated

*e-mail: sao@dec.feis.unesp.br, josear@ufscar.br

Table 1. Composition formulated for the refractory castable without cement.

Raw materials	wt. (%)
Electrofused aluminas 10/36 to 200	61.27
Calcined aluminas 3000 to 1000	38.73
Total	100.00

using the PSDesigner program, version 2.0.0 developed by GEMM[30]. The maximum temperature applied during sintering was 1360 °C.

The test specimens were prepared in the form of plates. The final size of the test specimen was defined considering not only the maximum size of the particles (to ensure the analysis of an area representative of the microstructure) but also the unfeasibility of sintering and testing very large pieces of refractory castable.

Two distinct sets of test specimens were prepared, one with a thickness three times the diameter of the largest particle and the other with a thickness five times that diameter. Both sets of test specimens were formulated with a maximum particle size of 2 mm.

The dimensions of the two sets of test specimens are given in Table 2. The proportions of the two sets were t: W: L equal to 1: 10: 20, where t is the thickness, W the width and L the length of the test specimen. The specimens were machined and notches were made with nominal lengths of 12, 24, 36, 48, 60 and 72 mm in the small test specimens (hereinafter referred to as CP_p), and of 20, 40, 60, 80, 100 and 120 mm in the large specimens (hereinafter referred to as CP_g).

In both the small and large test specimens, the notch length corresponded to 10, 20, 30, 40, 50 and 60% of L, i.e., the relative notch size was $0.1 \leq a_0/L \leq 0.6$, where a_0 represents the notch length.

With regard to notch size, experiments conducted by Shetty & Virkar[31] demonstrated that the equation to obtain K_I, considering the double-torsion geometry, overestimates K_I for short notch lengths and underestimates it for long lengths. The authors proposed the following operational notch extension: $0.21 < a_0/L < 0.58$ and $0.27 < a_0/L < 0.47$ for the test specimen dimensions t: W: L of 1: 31.25: 75 and 1: 50: 75, respectively. According to the authors, at these extensions, the K_I deviations fell within 5%.

Pletka et al.[17] also proposed a notch extension, $0.18 < a_0/L < 0.78$, as illustrated in Figure 1.

In an analysis of stress in a double-torsion test specimen using finite elements, Trantina[15] considered a sloping crack propagation front, deducing another acceptable operational extension. However, this analysis did not explore the influence of the groove and of the initial notch. The relative dimensions of Trantina's[15] test specimen were 1: 10: 20 for t, W and L, respectively, which are the same dimensions as those used in the present work.

The test specimens of this study also had a 1 mm deep and 3 mm wide groove centered along their length, on the face under tensile stress, in order to induce a straight path for the crack.

Further details of the preparation of the material and samples are given in Albuquerque[32].

3. Experimental Procedure

All the tests were carried out in an MTS series 810/458 servo-hydraulic testing machine.

The tests to determine the Young's modulus, E, were carried out in a three-point bending configuration. The calculations followed the procedure proposed by Hübner & Schuhbauer[33], in which a prismatic test specimen with a rectangular section is loaded twice, once with the largest dimension and again with the smallest dimension of the transverse section supported on the rollers. In both loadings, the test remains in the elastic region. The two load vs. displacement curves are subtracted from each other and the modulus is calculated independently of the influence of the test accessories. The value of E was transformed into G, the shear modulus, by applying the elastic relationship $G = E/[2(1+\nu)]$, assuming the Poisson's ratio, ν, equal to 0.25.

Table 2. Dimensions of the test specimens.

Test specimen sets	t (mm)	W (mm)	L (mm)
CP_p	6	60	120
CP_g	10	100	200

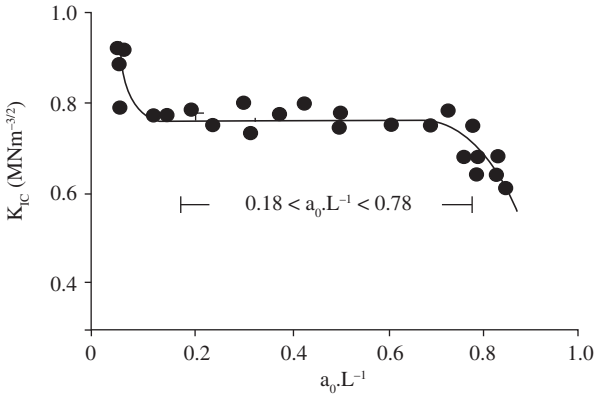

Figure 1. K_{IC} measured in toluene for sodium-lime-silica glass as a function of the $a_0.L^{-1}$ ratio in double-torsion tests[17].

The physical properties of apparent porosity, apparent specific mass of the solid part, and apparent specific mass of the sintered material were obtained by the Archimedes method, ABNT[34] and Wilson et al.[35].

Three methods are used for the double-torsion test, each with different loading conditions: the constant load rate (CLR)[5], the constant displacement rate (CDR)[8], and the load relaxation (RLX) method[8]. The method adopted in this work was CDR, which is more suitable for obtaining the R-curve.

The double-torsion method was utilized both to study the compliance calibration curve and to obtain the load-displacement curves and R-curves. Details of this test are given by Albuquerque & Rodrigues[36].

The equations associated with the double-torsion test are based on the assumption that the test specimen is a thin plate[10]. Evans et al.[37] and Atkinson[38] demonstrated, experimentally, that W should be 12-fold greater than t, while Pletka et al.[17] suggested that the test specimen's length, L, should be double that of the value of W. For these authors, the size of the double-torsion test specimen should follow the ratio of $12t \leq W \leq L/2$. However, as mentioned earlier, Shetty & Virkar[31] studied this test specimen geometry with the dimensions of t: W: L of 1: 31.25: 75 and 1: 50: 75, while Trantina[15] analyzed stress in a double-torsion test specimen with relative dimensions of 1: 10: 20 for t, W and L, respectively, the same proportions as those used in the present study. By reducing the ratio of W to t, one can obtain smaller test specimens that are easier to handle, sinter and test in the laboratory.

To reduce the ratio of W to t requires using a thickness correction factor in the expressions deduced for the stress intensity factor, K_I, and for the slope of the straight line of the compliance, B, obtained analytically from the double-torsion test[16,17], as shown in the equations below.

$$K_I = P \cdot W_m \left(\frac{3(1+\nu)}{W \cdot t^3 \cdot t_n \cdot \varepsilon} \right)^{1/2}, \quad (1)$$

$$B = \frac{3 \cdot W_m^2}{W \cdot t^3 \cdot G \cdot \varepsilon}, \quad (2)$$

$$\varepsilon = 1 - 0.6302 \cdot \left(\frac{2 \cdot t}{W}\right) + 1.20 \cdot \left(\frac{2 \cdot t}{W}\right) \cdot \exp\left(\frac{\pi}{t}\right), \quad (3)$$

where ε is the correction factor as a function of the test specimen thickness defined by equation 3, P is the applied load, W_m is the distance between supports and t_n is the thickness after discounting the depth of the groove.

In this work, it was used the a_0/L ratio of 0.1, 0.2, 0.3, 0.4, 0.5, and 0.6 for the dimension of the notch. This range covered the extension recommended by Shetty & Virkar[31], $0.21 < a_0/L < 0.58$ and $0.27 < a_0/L < 0.47$ for the test specimen dimensions t: W: L of 1: 31.25: 75 and 1: 50: 75, and almost the entire extension proposed by Pletka et al.[17], $0.18 < a_0/L < 0.78$.

The double-torsion test also allows one to calculate the crack propagation velocity, using Evans & Wiederhorn's formula[39] expressed as:

$$V = \frac{dy/dt}{P \cdot B} \quad (4)$$

where dy/dt is the actuator's displacement velocity during the crack propagation test.

The R-curve was obtained by the double-torsion test, according to the equation below[32,36].

$$R_i = \frac{P_i^2 \cdot {W_m}^2 \cdot 3 \cdot (1+\nu)}{E \cdot W \cdot t^3 \cdot t_n \cdot \varepsilon}, \quad (5)$$

where i represents a random point of the load-displacement curve upon which the P_i value is read. Equation 5 presents R by the Linear Elastic Fracture Mechanics (LEFM) method, which establishes that $R=K_I^2/E$[40].

The value of a_i, considered the instantaneous length of the crack, was estimated from the compliance calibration curve for the material under study[32,36], and is written as:

$$a_i = a_0 + \Delta a_i = a_0 + \frac{C_i - C_0}{B} \quad (6)$$

where C_0 is the initial compliance of the notched specimen, C_i is the compliance for the crack length a_i, and Δa_i is the variation of the length of the crack up to the instant i.

4. Results and Discussion

4.1. Physical properties and elastic moduli

An average value of 128 GPa, with a standard deviation of 2 GPa, was found for Young's modulus, E, of this material following the aforementioned method. The value of ν = 0.25 was adopted for the estimation of the shear modulus, G = 50 GPa.

The values of apparent density, Pa, apparent specific mass of the solid part, M_{eas}, and of the apparent specific mass, M_{ea}, are given in Table 3.

Table 3. Physical properties of the material under study.

Pa (%)	M_{eas} (g.cm^{-3})	M_{ea} (g.cm^{-3})
16.6 + 0.7	3.71 ± 0.02	3.09 ± 0.01

4.2. Compliance

The equations for the compliance of the large, C_g, and small, C_p, test specimens extracted from the corresponding calibrations curves are:

$$C_g = 1.41 \cdot 10^{-6} a + 2.12 \cdot 10^{-7} \quad (7)$$

and

$$C_p = 5.47 \cdot 10^{-6} a + 4.23 \cdot 10^{-7} \quad (8)$$

where C_g and C_p in units of m/N for the crack length, a, in units of m. In Equations 7 and 8, a represents the size of the crack or of the notch, a_0, whenever that is the case. These calibration curves are depicted in Figure 2.

Table 4 lists the theoretical values of B obtained from Equation 2 and, for purposes of comparison, also shows the experimental values obtained from the calibration curve equations (Equations 7 and 8), corresponding to Figure 2.

The experimental value of B of the large test specimens corresponds to 26% of the value of B for the small specimens. Comparing this value against the mean theoretical value of B (equation 2), calculated from the real dimensions of the test specimen, indicates that the B of the large test specimen corresponds to 30% of the value of B of the small specimen. It can be stated that the real difference in the B value of the two test specimen sizes is close to the value predicted theoretically. Therefore, the value of B of the small test specimen's calibration curve is representative.

4.3. Validity range of the notch length

In this study, the a_0/L ratio values of 0.1, 0.2, 0.3, 0.4, 0.5 and 0.6 were used for the two test specimen sizes, where a_0 is the notch length.

The test specimens with longer notch lengths showed a shorter extent of stable crack growth. This led to the recording of fewer points for the P x d curve and, hence, to inaccuracy in the subsequent analyses of these curves. Therefore, only the curves with notch lengths with a_0/L of 0.1 and 0.2 will be shown here.

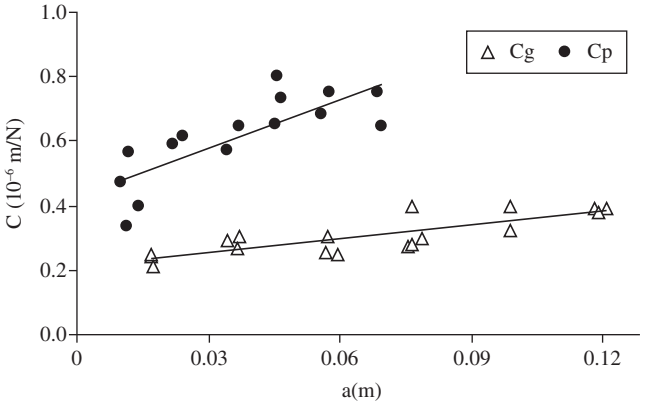

Figure 2. Compliance calibration curves, C, versus crack (or notch) length, a, for large and small test specimens.

Table 4. Theoretical and experimental values of B of the castable under study for the two test specimen sizes.

Equations	B (N^{-1})	
	Small test specimens	Large test specimens
Theoretical, Equation 2	4.08 x 10^{-6} ±4.60 x 10^{-8}	1.22 x 10^{-6} ±9.03 x 10^{-8}
Equations 7 and 8	5.47 x 10^{-6}	1.41 x 10^{-6}

As mentioned in a previous paper by those authors[36], again, for this material, the use of short notch lengths is also recommended. In that work, the lowest a_0/L ratios presented the best results for the R-curve analysis, although, according to Shetty & Virkar[31], the lowest a_0/L ratio would be 0.2 for the 1:31.25:75 for the proportion of dimensions of the test specimen and, according to Pletka et al.[17], a_0/L should be higher than 0.18 and lower than 0.78. The present work indicated that very long notch lengths ($a_0/L > 0.3$) do not allow for sufficient extension of stable propagation, which is a disadvantage for obtaining R-curves. This limitation is due not to the validity of the K_I equation, but simply to the representative stable extension of the crack.

4.4. Analysis of the validity range of the notch length

In order to ascertain, according to Shetty & Virkar[31] and Pletka et al.[17] (Figure 1), whether the relative length of the crack, a_0/L, used in the present study is valid, the fracture toughness, K_{IC}, was substituted by the maximum stress intensity factor, K_{Imax}. This parameter is the K_I value calculated for the maximum load value of the P x d curve. This was made because the test is slow and leads not to catastrophic break but to stable propagation. Figure 3 shows K_{Imax} as a function of a_0/L for the two sizes of samples.

Figure 3 indicates that K_{Imax} drops 27% from the highest to the lowest value of this magnitude in the interval of a_0/L of 0.1 to 0.4 for the large test specimens and 37% for the small test specimens. Shetty & Virkar[31] recommended the value of 5% for different notch length. However, the dispersion for the same notch length, a_0/L of 0.3 for the large test specimens, was 25% and for the small test specimen the dispersion for a_0/L of 0.2, was 27% in the material used in this study. This dispersion must be associated with the coarse microstructure due to the particles of 2 mm in diameter.

According to Sakai[41] and Lemaistre[42], materials with coarse microstructures show greater dispersion than materials whose microstructure is finer, denser and more homogeneous.

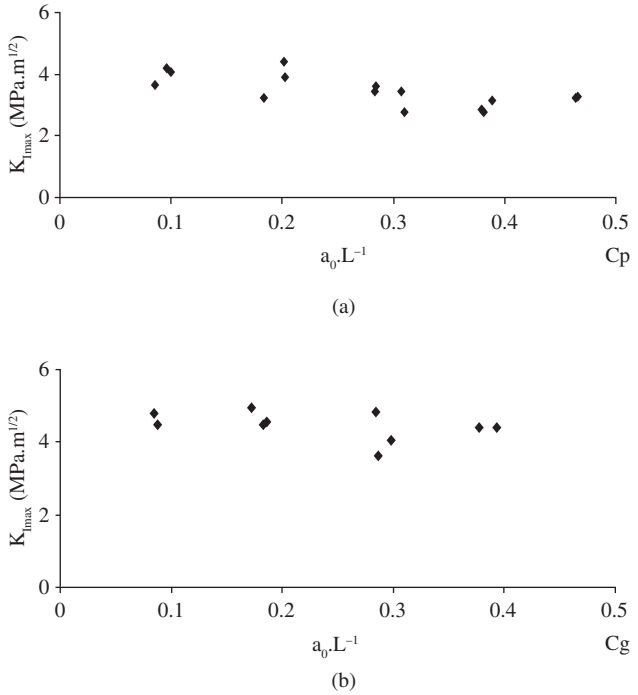

Figure 3. Maximum stress intensity factor, K_{Imax}, versus a_0/L: a) small test specimens; and b) large test specimens.

Working with castable and obtaining R-curves by the four-point bending test, Lemaistre[42] noted dispersion in the R-curves and in the maximum R values of up to approximately 50%, as illustrated in Figure 4. He also observed that this dispersion increased along with the particle size. In Figure 4, the MChZ5 with the largest particle size (7 mm) was the castable that showed the greatest dispersion.

Taking the maximum value of R, R_{max}, found by Lemaistre[42] (Figure 4), transforming it into K_{Imax} using Irwin's equation[40], $R = K^2/E$, and substituting K_{IC} with K_{Imax}, yields a dispersion of about 30% of the K_{IC} values for the MChZ5 castable. This value is much closer to the value found in the present study.

The variation was slightly higher in the small test specimens. The highest value of K_{Imax} was 35% higher than the lowest value and the dispersion for the same notch length, a_0/L of 2.4, was 25%.

Pletka et al.[17] also made a study of this criterion of crack (or notch) validity range and how it relates to the geometry of the test specimen, and concluded that further studies about this criterion were still needed.

4.5. Double-torsion test

In the double-torsion test, the P x d graph depicts the region of elastic deformation (beginning of the curve) and the region of stable crack propagation (where the points begin to deviate from the straight line of the elastic region, including the plateau and the break (abrupt load drop). For test specimens with notches in the a_0/L range of 0.5 and 0.6, the break occurred before the material left the elastic region, and in these cases, stable crack propagation did not occur and the break load was much lower than the others. The R-curve was not obtained with these tests.

Figure 5 gives examples of P x d curves for large test specimens with nominal notch lengths of 2 cm and for small test specimens with nominal notch lengths of 1.2 cm. The depths of the notches in the two specimen sizes were proportional, i.e., 10% of L. Figure 5 also shows the corresponding R-curves.

Figure 6 gives the same information as Figure 5, but for large test specimens with nominal notch lengths of 4 cm and for small test specimens with nominal notch lengths of 2.4 cm. The corresponding R-curves are also shown.

For a_0 values equal to 30 and 40% of L there were few points of stable propagation, hampering the analysis of the results, which are therefore not shown here.

The R-curves obtained by the double-torsion test for both test specimen sizes revealed the same behavior in terms of shape. This

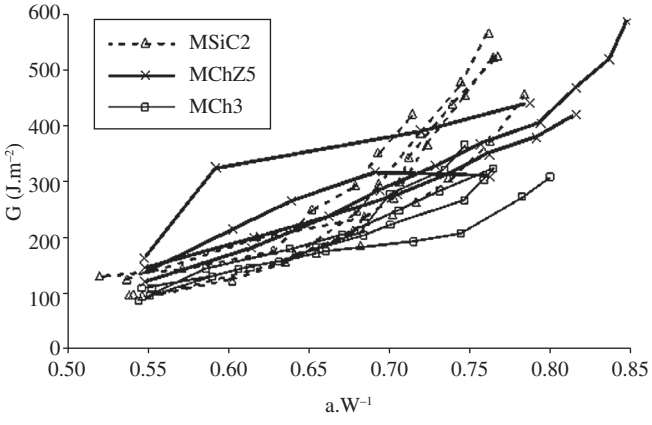

Figure 4. Dispersion of the R-curves obtained by Lemaistre (1998) for different castables. Here, a/W is equivalent to the a_0/L of this study.

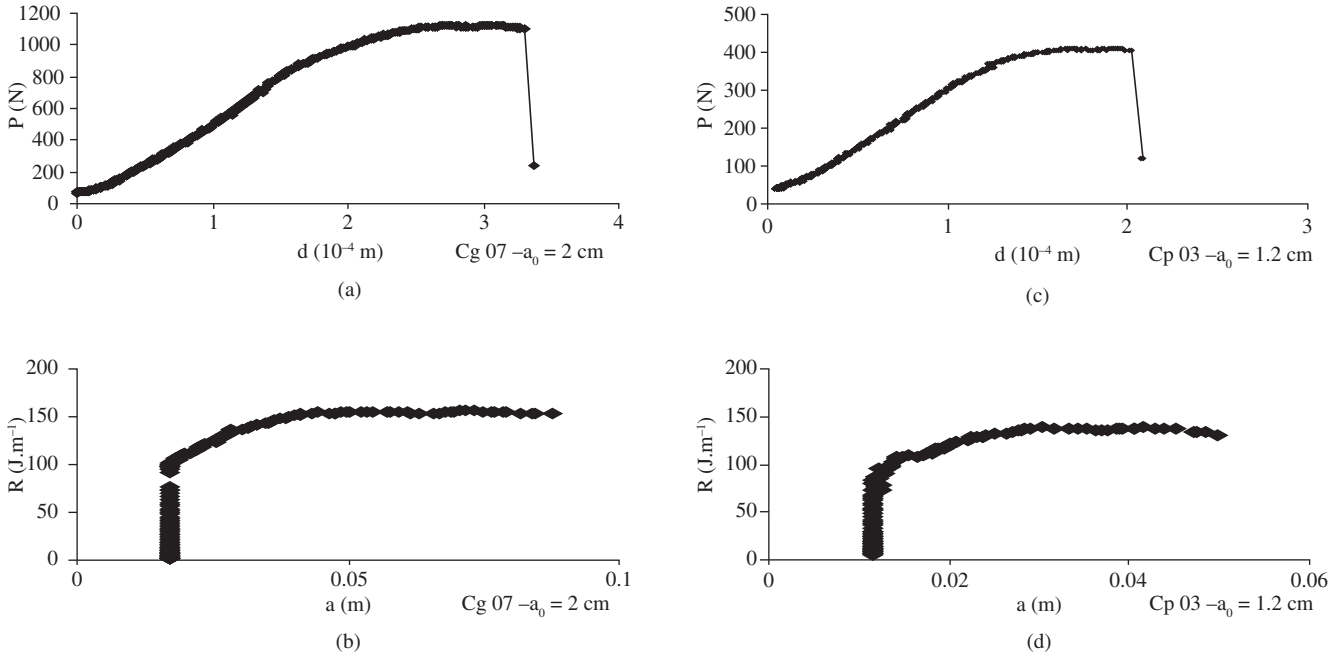

Figure 5. Graphs a-b) correspond to the large test specimens (CP_g), with $a_0 = 2$ cm. Graphs c-d) correspond to the small test specimens (CP_p), with $a_0 = 1.2$ cm. Graphs a, c) are P x d graphs, while b,d) are the corresponding R-curve graphs.

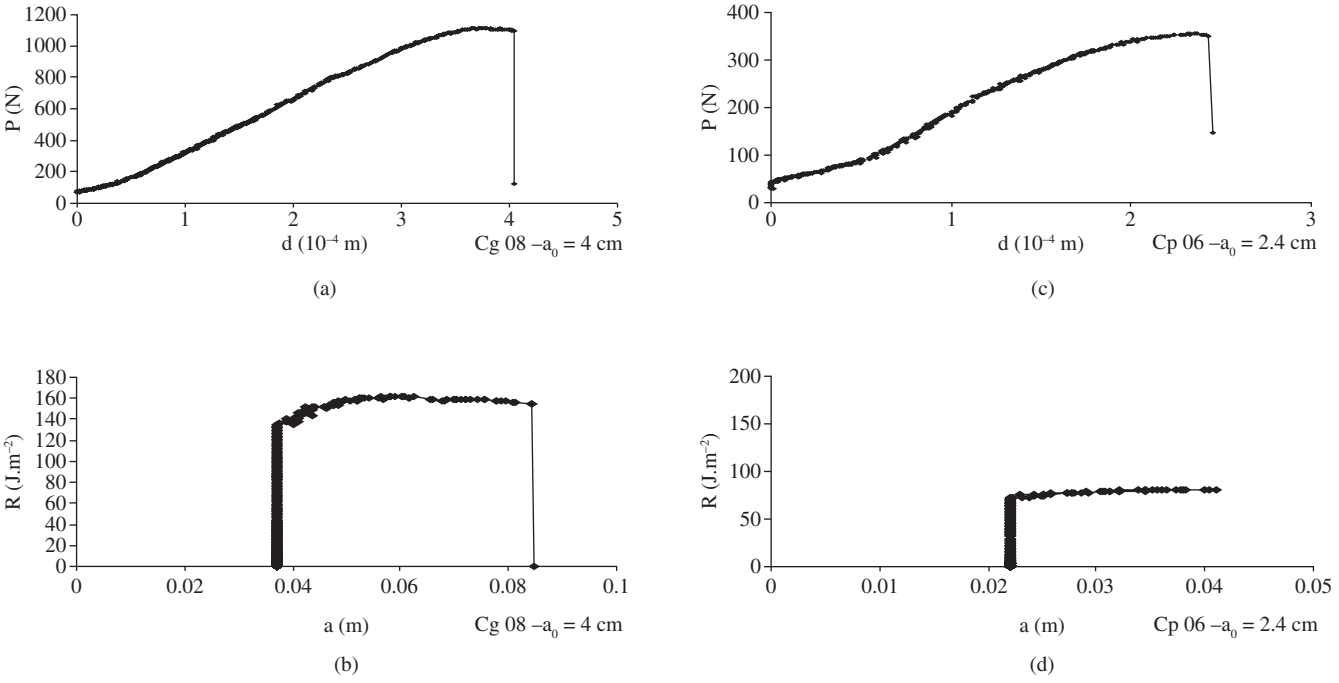

Figure 6. Graphs a-b) correspond to the large test specimens (CP_g), with $a_0 = 4$ cm. Graphs c-d) correspond to the small test specimens (CP_p), with $a_0 = 2.4$ cm. Graphs a, c) are P x d graphs, while b, d) are the corresponding R-curve graphs.

behavior was already expected for alumina in the initial state of crack expansion, i.e., an increase in strength with the growth of the crack, followed by a plateau[41].

To evaluate the reliability of the R values obtained, the comparison criterion of the mean R value, $\overline{R}$, and the work of fracture, γ_{wof}, multiplied by 2, were used according to Nakayama[43]. The work of fracture was calculated up to the ultimate point of the stable propagation. The value of $\overline{R}$ was obtained by the arithmetic average of the R values in the stable propagation portion of the crack, i.e., the values of R for which the values of a begin to increase (Figures 5b, 5d, 6b and 6d). The equations used to calculate the values of $\overline{R}$ and γ_{wof} are given in Albuquerque & Rodrigues[36] and Albuquerque[32]. Table 5 shows the values of $\overline{R}$ and $2{\cdot}\gamma_{wof}$ obtained in this work.

The large test specimens showed higher mean values of $\overline{R}$ and $2{\cdot}\gamma_{wof}$, as indicated in Table 5.

When test specimens are of the same material, the behavior of the R-curve, in terms of the values of $\overline{R}$ and $2{\cdot}\gamma_{wof}$, is showing a dependence on the size of the test specimen. Moreover, $\overline{R}$ and $2{\cdot}\gamma_{wof}$ are dependent on a_0, as also indicated in Table 5. This table reveals a tendency for $\overline{R}$ and $2\gamma_{wof}$ to diminish as a_0 increases in both large and small test specimens. Only the crack length a_0 = 8 cm or a_0/L = 0.4 in the large test specimens did not show this tendency. This was probably due to the wide dispersion in the case of the test specimens with a_0 = 6 cm (Table 5).

Table 5 also shows that both test specimens sizes presented $\overline{R} > 2{\cdot}\gamma_{wof}$.

4.6. Critical crack length

In the double-torsion test, in both the material studied here and a material studied by Albuquerque & Rodrigues[36], catastrophic propagation occurred after a certain length of stable propagation, as shown in Figure 5a, for example. The crack length at which catastrophic break of the specimen occurs was defined as the critical crack length, a_c. The value of a_c is obtained from equation 6 for the value of C_i at the point corresponding to catastrophic rupture, when the load drops abruptly.

Figure 7 shows the critical crack length, a_c, vs. the notch length, a_0. As can be seen, the notch length did not affect the critical crack length in either the large or the small test specimens. The horizontal lines in Figure 7 indicate the mean values of a_c of 8.5 cm for the large test specimens and of 5.0 cm for the small ones. It is interesting to note that these mean values represent 42% of the total length of the test specimens, both for the small 12-cm-long test specimens and the large 20 cm-long ones. It can therefore be stated that the critical crack length was representative for the small test specimen. With three other materials[32,36], obtained that the catastrophic rupture occurred at 71, 45 and 38% of the total length of the test specimens. It can therefore be stated that, for the materials studied by the authors, the critical crack length varies according to the material and not to the dimensions of the test specimen.

Figure 8 shows the extent of stable crack propagation, Δa_{st}, as a function of notch size, where Δa_{st} is defined as $a_c - a_0$. Figure 8 confirms that the shorter the notch length the greater the extent of stable propagation. This was true for both test specimen sizes.

4.7. Crack propagation velocity

Figure 9 illustrates the mean theoretical crack propagation velocity, V, calculated from Equation 4 (with the value of B obtained from

Table 5. Values of $\overline{R}$ and $2{\cdot}\gamma_{wof}$ for the material under study.

Large test specimens			Small test specimens		
a_0 (cm)	$\overline{R}$ (J/m^2)	$2{\cdot}\gamma_{wof}$ (J/m^2)	a_0 (cm)	$\overline{R}$ (J/m^2)	$2{\cdot}\gamma_{wof}$ (J/m^2)
2	174 ± 20	133 ± 17	1.2	128 ± 20	113 ± 18
4	164 ± 15	118 ± 18	2.4	89 ± 11	86 ± 12
6	129 ± 33	108 ± 13	3.6	83 ± 15	69 ± 9
8	136 ± 14	143 ± 63	4.8	64 ± 8	55 ± 11
Mean value	151 ± 18	126 ± 13	Mean value	96 ± 23	87 ± 21

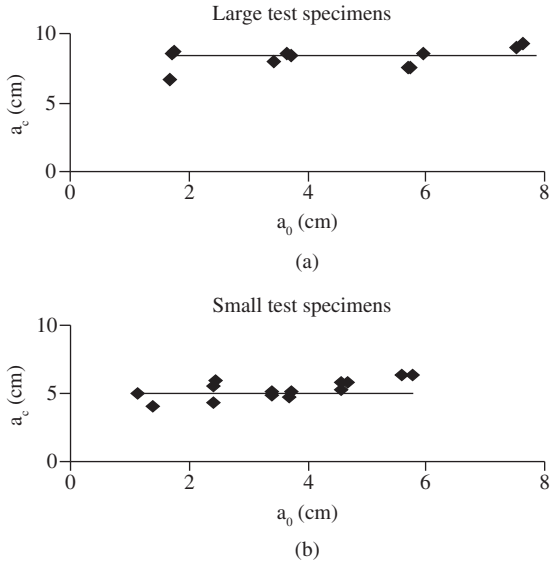

Figure 7. Critical crack length, a_c, versus notch length, a_0; a) for large test specimens, and b) for small test specimens.

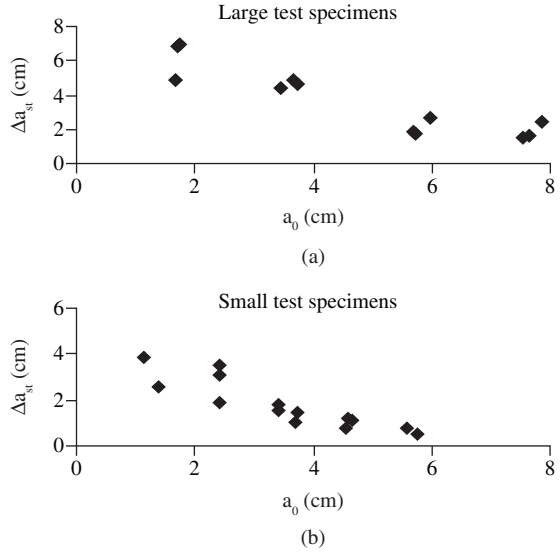

Figure 8. Extent of stable crack propagation, $\Delta a_{st} = a_c - a_0$, versus notch length, a_0; a) for large test specimens; and b) for small test specimens.

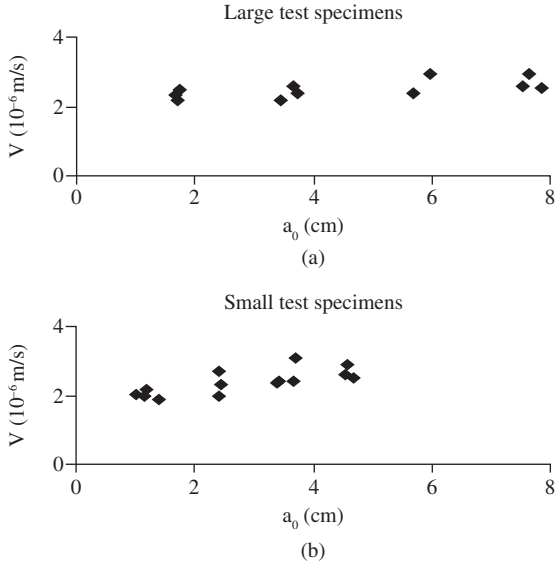

Figure 9. Mean theoretical crack propagation velocity, V, versus a_0; a) large test specimens; and b) small test specimens.

Equation 2), versus notch size. As can be seen in this figure, the mean crack propagation velocity did not vary significantly with the notch length in either of the two test specimen sizes, and in both sizes the propagation velocity remained between 2×10^{-6} and 3×10^{-6} m/s.

4.8. Final remarks

The two castable test specimen sizes showed no variation in the relative critical crack length. It was found that the small and large test specimens presented the same a_c value in relation to the length of the test specimen, i.e., approximately 42%.

The analytical and experimental values of B for the double-torsion test, slope of the straight line of compliance calibration curve, were mutually congruent.

When one compares the values of B for the two test specimen sizes, one finds that the theoretical value of B of the large test specimen corresponded to 30% of the value of B of the small one, and the experimental value of B of the large test specimen corresponded to 26% of the value of B of the small one.

The mean theoretical crack propagation velocity was approximately the same for the two test specimen sizes (values of 2×10^{-6} to 3×10^{-6} m/s).

There was little or no stable propagation when the notch length was close to the critical crack length, and catastrophic break occurred. In this situation, the P x d curve presented elastic deformation (load increase) and the test specimen broke soon after ultimate loading, when the load fell abruptly. For notches shorter than the critical crack length, the P x d curve showed the expected behavior, i.e., one portion of the curve corresponding to elastic strain, the other to stable crack propagation (subcritical growth and approximately constant load) and catastrophic rupture.

It seems that, for the R-curve, the test specimen really must have a section of crack propagation that involves an area representative of the microstructure; otherwise, the results one obtains for its evaluation are questionable. This is a major advantage of the geometry of the double-torsion test specimen, in which the crack propagates along the specimen's largest dimension.

The R-curves for the two different test specimen sizes initially showed a slight increase in R, tending toward a plateau, which is in agreement with the behavior predicted theoretically for alumina. Therefore, with respect to the shape of the R-curve, there was no discrepancy between the results of the small and large test specimens. In other words, the curves tended to a plateau, which did not occur when the authors applied this test to other materials. In those cases, the R-curves showed a decline in the load-displacement curve, which was reflected in the R-curve[32,36]. However, the values of $\overline{R}$ and $2 \cdot \gamma_{wof}$ of the small test specimens were lower than those of the large ones. Therefore, the values of $\overline{R}$ and γ_{wof} proved to be dependent on the size of the test specimen. Both test specimen sizes presented the same ratio of $\overline{R} > 2 \cdot \gamma_{wof}$.

5. Conclusions

The critical crack length did not vary with the notch length. The absolute and relative values of critical crack length did not vary with the notch length or with the test specimen dimensions.

The difference between the experimental values of B for the two test specimen sizes is theoretically predictable.

The mean theoretical crack propagation velocity of the two test specimen sizes showed no significant difference.

For notch lengths close to the critical crack length, there is insufficient stable propagation to allow for an evaluation of the R-curve.

The two test specimen sizes showed mutual congruence of the R-curve shape.

The values of $\overline{R}$ and of $2 \cdot \gamma_{wof}$ proved dependent on the size of the test specimen.

In the geometry of the double-torsion test, a thickness three times that of the largest grain demonstrated that the test specimen showed a qualitative behavior of stable crack propagation representative of various aspects of the material. However, an analysis of the values of $\overline{R}$ and $2 \cdot \gamma_{wof}$ revealed that these values were lower for the small test specimens.

It is clear that the subject under discussion deserves further study, since this work presented results that were positive from several standpoints.

Acknowledgements

The authors gratefully acknowledge FAPESP (Process # 2001/04324-8), CNPq (Process # 304980/2003-0, 301073/2006-6, 470504/2004-8 and 143336/1998-3), and PROPE-UNESP for their financial support, and Alcoa Alumínio S.A., Poços de Caldas-MG, Brazil, for its donation of the raw materials used in this research.

References

1. Nara Y, Kaneco K. Study of sub critical crack growth in andesite using the double-torsion test. *International Journal of Rock Mechanics and Mining Sciences.* 2005; 42(4):521-530.
2. Outwater JO, Gerry DJ. *On the fracture energy of glass.* NRL Interim Contract Report, Contract NONR 3219 (01) (x), AD 640848. Burlington: University of Vermont; Aug. 1966.
3. Outwater JO, Gerry DJ. On the fracture energy, rehearing velocity and fracture energy of cast epoxy resin. *Journal of Adhesion.* 1969; 1:290-298.
4. Outwater JO, Austin LE. Effect of external hydrostatic pressure on damage glass hydrospheres. In: ASTM International (Ed.). *Materials Performance and the Deep Sea*. Philadelphia: American Society for Testing and Materials; 1969. p. 41-54.
5. Kies JA, Clark ABJ. Fracture propagation rates and times to fail proof stresses in bulk glass. In: Pratt PL (Ed.). P*roceedings of the Second International Conference on Fracture.* Brighton, England, London: Chapman and Hall Ltd.; 1969. p. 483-491.
6. Beachem CD, Kies JA, Brown BF. Constant K specimen for stress corrosion cracking tests. *Materials Research and Standards*. 1970; 11(4):30.
7. Outwater JO, Murphy MC. On the fatigue of epoxy resin. In: *Proceedings of the Twenty Six Annual Technology Conference Reinforce Plastic*; 1971; Washington, DC. Washington: Compos Division Proceedings; 1971. p. 6.
8. Evans AG. A method for evaluating the time-dependent failure characteristics of brittle materials – and its application to polycrystalline alumina. *Journal of Materials Science*. 1972; 7(10):1137-1146.
9. Evans AG. A simple method for evaluating slow crack growth in brittle materials. *International Journal of Fracture*. 1973; 9(3):267-275.
10. Williams DP, Evans AG. A simple method for studying slow crack growth. *Journal of Testing and Evaluation*. JTEVA. 1973; 1(4):264-270.
11. McKinney KR, Smith HL. Method of studying subcritical cracking of opaque materials. *Journal of the American Ceramic Society*. 1973; 56(1):30-32.
12. Outwater JO, Murphy MC, Kumble RG, Berry JT. Double Torsion Technique as a universal fracture toughness test method. In: ASTM (Ed.). *Fracture toughness and slow-stable cracking*. Philadelphia: American Society for Testing and Materials; 1974. p. 127-138.
13. Weidmann GW, Holloway DG. Slow crack propagation in glass. *Physics and Chemistry of Glasses*. 1974; 15(5):116-122.
14. Virkar AV, Johnson DL. Fracture behaviour of ZrO//2-Zr Composites. *Journal of the American Ceramic Society*. 1976; 59(5-6):197-200.

15. Trantina GG. Stress Analysis of the double-torsion specimen. *Journal of the American Ceramic Society.* 1977; 60(7-8):338-341.
16. Fuller-Jr ER. *An Evaluation of Double Torsion Testing – Analysis, Fracture Mechanics Applied to Brittle Materials*. ASTM STP 678. S.W. Freiman (Ed.). American Society for Testing and Materials; 1979. p. 3-18.
17. Pletka BJ, Fuller-Jr ER, Koepke BG. *An Evaluation of Double Torsion Testing – Experimental, Fracture Mechanics Applied to Brittle Materials*. ASTM STP 678. S.W. Freiman (Ed.). American Society for Testing and Materials; 1979. p. 19-37.
18. Chevalier J, Saadaoui M, Olagnon C, Fantozzi G. Double-Torsion Testing a 3Y-TZP Ceramic. *Ceramics International.* 1996; 22(2):171-177.
19. Ciccotti M, Gonzato G, Mulargia F. The double torsion loading configuration for fracture propagation: an improved methodology for the load relaxation at constant displacement. *International Journal of Rock Mechanics & Mining Sciences.* 2000; 37(7):1103-1113.
20. Ciccotti M, Negri N, Gonzato G, Mulargia F. Practical Application of an Improved Methodology for the Double-Torsion Load Relaxation Method. *International Journal of Rock Mechanics & Mining Sciences.* 2001; 38(4):569-576.
21. Ebrahimi ME, Chevalier J, Fantozzi G. R-Curve Evaluation and Bridging Stress Determination in Alumina by Compliance Analysis. *Journal of the European Ceramic Society*. 2003; 23(6):943-949.
22. Pçdzich Z. The reability of particulate composites in the TZP/WC system. *Journal of the European Ceramic Society.* 2004; 24(12):3427-3430.
23. Aza AH, Chevalier J, Fantozzi G. Slow-crack-growth behaviour of zirconia-toughened alumina ceramics processed by different methods. *Journal of the American Ceramic Society.* 2003; 86(1):115-120.
24. Radovic M, Lara-Curzio E. Mechanical properties of tape cast nickel-based anode materials for solid oxide fuel cells before and after reduction in hydrogen. *Acta Materialia.* 2004; 52(20):5747-5756.
25. Zhu P, Lin Z, Chen G, Kiyohiko I. The predictions and applications of fatigue lifetime in alumina and zirconia ceramics. *International Journal of Fatigue.* 2004; 26(10):1109-1114.
26. Davies AR, Field JE, Takahashi K, Hada K. Tensile and fatigue strength of free-standing CVD diamond. *Diamond and Related Materials*. 2005; 14(1):6-10.
27. Deville S, Asan ElA, Chevalier J. Atomic force microscopy of transformation toughening in ceria-stabilized zirconia. *Journal of the European Ceramic Society.* 2005; 25(13):3089-3096.
28. Benaqqa C, Chevalier J, Saadaoui M, Fantozzi G. Slow crack growth behaviour of hydroxyapatite ceramics. *Biomaterials*. 2005; 26(31):6106-6112.
29. Pçdzich Z, Wajler C. Slow crack propagation in Y-TZP/metal composites. *Journal of the European Ceramic Society*. 2006; 26(4-5):679-682.
30. Pileggi RG, Ortega FS, Morábito R, Vendrasco S, Pandolfelli VC. Desenvolvimento e aplicação de um software que automatiza o processo de combinação de matérias-primas na obtenção de produtos cerâmicos. *Cerâmica*. 1998; 44(289):189-195.
31. Shetty DK, Virkar AV. Determination of the useful range of crack length in double torsion specimens. *Journal of American Ceramic Society.* 1978; 61(11):93-94.
32. Albuquerque MCF. *Estudo do Ensaio de Dupla-Torção para Determinação da Curva-R de Concretos Refratários*. [Unpublished D. Phill Thesis]. São Carlos: Universidade Federal de São Carlos; 2003.
33. Hübner H, Schuhbauer H. Experimental Determination of fracture Mechanics Stress Intensity Calibration in Four-point Bending. *Engineering Fracture Mechanics*. 1977; 9(2):403-410.
34. ABNT – NBR 6220. *Material refratário – determinação da massa específica aparente, massa específica aparente da parte sólida, absorção de água, porosidade aparente e total.* Rio de Janeiro: ABNT; 1980.
35. Wilson MA, Carter MA, Hoff WD. British standard and RILEM water absorption tests: a critical evaluation. *Materials and Structures.* 1999; 32(222)571-578.
36. Albuquerque MCF, Rodrigues JA. Characteristics of the double-torsion test to determine the R-curve of ceramic materials. *Materials Research.* 2006; 9(4):361-368.
37. Evans AG, Linzer M, Russell LR. Acoustic emission and crack propagation in polycrystalline alumina. *Materials Science and Engineering*. 1974; 15(2-3):253-261.
38. Atkinson BK. Technical note. Fracture toughness of Tennessee Sandstone and Carrara Marble using the double torsion testing method. *International Journal of Rock Mechanics and Mining Science Geomech Abstracts.* 1979; 16:49-53.
39. Evans AG, Wiederhorn SM. Crack propagation and failure prediction in silicon nitride at elevated temperatures. *Journal of Materials Science*. 1974; 9(2):270-278.
40. Irwin GR. Analysis of stress and strain near the end of a crack. *Journal of Applied Mechanics*. 1957; 24:361.
41. Sakai M. Fracture Mechanics of Refractory Materials. *Taikabutsu Overseas*. 1987; 8(2):4-12.
42. Lemaistre H. *Étude des propriétés thermomécaniques de divers réfractaires*. [Unpublished D. Phill Thesis]. Lyon: École Doctorale Matériaux: Institut National de Sciences Appliquées; 1998.
43. Nakayama J. Direct Measurement of fracture energies of brittle heterogeneous materials. *Journal of American Ceramic Society.* 1965; 48(11):583-587.